

# Analysis of Mode I and Mixed Mode Stress Intensity Factors with Digital Image Correlation

ME EN 6960

Nik Benko, John Callaway, Nick Dorsett, Martin Raming

March 28, 2018

## Abstract

Failure in a material is often dependent on the presence of flaws within the part. One form these flaws take is in cracks which appear along the edge of a part. In this experiment, Digital Image Correlation was used to analyze the displacement field of a thin sheet of polymethyl methacrylate during a Single Edged Notch Bend test. This test was then repeated using an asymmetric three point bend configuration to produce a set of data under mixed mode loading. The Westergaard stress function solution for an edge crack was used to compute the stress intensity factors for each data set, and the Mode I data was compared to an analytical solution calculated with strength of materials equations.

## 1 Introduction

In practice, the failure load of a macroscopic material is lower than the predicted failure load of the individual atomic bonds of the material. This occurs because geometric features, such as cracks, cause stress concentrations which magnify the effect of applied loads. Classical strengths of materials equations are useful for producing general solutions to problems, but in order to analyze specific cases in detail, Linear Elastic Fracture Mechanics (LEFM) is used instead. LEFM assumes that a crack is a free surface within

the surrounding stress field, the elastic solution surrounding this crack is based on a stress intensity factor  $K$ , and that the stress on the crack tip can be used to predict the crack propagation. Furthermore, the area surrounding a crack consists of three major parts. The first part, consisting of the crack tip, is a region of plastic deformation at which it is not valid to use LEFM due to the plastic deformation. The second region is the linear elastic region, where LEFM is applied in describing the stress state of the material. The third section is the far-field where the stress state is no longer affected by the presence of the crack. By analyzing the second region, information on the stress intensity factor can be determined for a variety of loads.

In previous works, such as that of Parnast et al, strain gauges were used to capture displacement around crack tips [1]. While strain gauges are useful in providing displacement data, they are only valid over the region directly underneath the gauge, limiting the information provided. Optical techniques, however, can be used to provide the full-field displacement data surrounding a crack. Through analyzing the contours present in full-field data, it can be determined what mode(s) in which the crack is loaded. Digital image correlation is an attractive method for measuring these displacement fields because it is applicable on most materials, does not require particularly complicated equipment, and is easy to set up and use. The usefulness of DIC for analysis of cracks has been shown in works such as Zhang et al where DIC was successfully used to analyze mixed mode loads to calculate stress intensity factors [2].

This paper describes the use of Digital Image Correlation (DIC) to capture displacement field data around a crack tip when it undergoes pure Mode I loading and mixed Mode I and Mode II loadings in a Single Edged Notch Bend (SENB) test. Using this information, the stress intensity factors are calculated using the Westergaard stress function solution for both Mode I and mixed mode loads [3]. These calculated stress intensity factors from LEFM are then compared to the analytical solution for the given loading scenario.

## 2 Methods

### 2.1 Experimental Techniques

#### 2.1.1 Digital Image Correlation

DIC is a commonly used optical technique to measure full-field displacements and rotations by capturing a sequence of images of a smooth surface during loading. Using two cameras, these measurements can be taken in 3D. If only 2D measurements are needed, as in this experiment, only one camera is required. An area of interest within the images is selected and then divided into sections known as subsets. Each subset is made up of the same number of pixels. A template matching function is used to correlate the subsets from the deformed images to a reference image within the DIC algorithm. By corresponding each pixel to an actual unit of length, deformations and rotations can then be tracked [4].

For the DIC algorithm to be effective, each subset must contain enough unique features. These features are related to contrast or pixel values within each subset. A high-contrast uniform granular surface is desired to create such usable features. In practice this is known as a speckle pattern. An effective speckle pattern consists of uniformly dispersed speckles of unique shapes and sizes. The size of the speckles and number of subsets influence the accuracy of measurements thus, it is important to apply a proper speckle pattern [5].

#### 2.1.2 Experimental Determination of Displacement Fields

Mode I displacement fields can be obtained by symmetrically loading a SENB specimen. The geometry of the SENB specimen is given in Figure 2. Alignment of the roller directly above the crack tip creates pure bending around the crack, which induces a predominantly Mode I crack opening, and therefore Mode I displacement fields. Mixed mode displacement fields can be obtained by inducing eccentricity in the SENB specimen. This can be done by moving one of the lower support rollers, creating a combination of bending (Mode I) and shear (Mode II) around the crack. This configuration is given in Figure 3.

### 2.1.3 Calculation of Stress Intensity Factors

Theoretical Mode I stress intensity factors ( $K_I$ ) can be calculated using the closed-form equation:

$$K_I = Y\sigma\sqrt{\pi a} \quad (1)$$

where  $\sigma$  is the far-field stress,  $a$  is the crack length and  $Y$  is a geometric factor specific to the loading configuration and specimen geometry. Using the solution developed in *The Stress Analysis of Cracks Handbook*, the stress intensity factor for the single edge notched bend specimen being examined is

$$K_I = \frac{P}{B\sqrt{w}} \left( \frac{\frac{3S}{w}\sqrt{\frac{a}{w}}}{2(1 + \frac{2a}{w})(1 - \frac{a}{w})^{1.5}} \right) \left[ 1.99 - \frac{a}{w} \left( 1 - \frac{a}{w} \right) \left[ 2.15 - 3.93 \left( \frac{a}{w} \right) + 2.7 \left( \frac{a}{w} \right)^2 \right] \right] \quad (2)$$

where  $P$  is the applied load,  $S$  is the support span,  $w$  is the specimen width,  $B$  is the specimen thickness and  $a$  is the crack length [6].

Experimental Mode I stress intensity factors can be found using experimental displacement fields. From the Westergaard solution, the displacements around the crack can be described by the following equations

$$u_x = \frac{K_I}{8\mu\pi} \sqrt{2\pi r} \left[ (2\kappa - 1) \cos\left(\frac{\theta}{2}\right) - \cos\left(\frac{3\theta}{2}\right) \right] \quad (3)$$

$$u_y = \frac{K_I}{8\mu\pi} \sqrt{2\pi r} \left[ (2\kappa + 1) \sin\left(\frac{\theta}{2}\right) - \sin\left(\frac{3\theta}{2}\right) \right] \quad (4)$$

where  $(r, \theta)$  are the polar coordinates of the point,  $\mu$  is the shear modulus,  $\kappa = \frac{3-\nu}{1+\nu}$ , and  $\nu$  is Poisson's ratio for the plane stress state of the experiment [3].

Mixed mode stress intensity factors can also be found using the experimental mixed mode displacement fields. The displacement field for a combined Mode I and Mode II loading configuration is the sum of

the displacements for each individual loading condition, as given by the following equations

$$u_x = \frac{K_I}{8\mu\pi} \sqrt{2\pi r} \left[ (2\kappa - 1) \cos\left(\frac{\theta}{2}\right) - \cos\left(\frac{3\theta}{2}\right) \right] + \frac{K_{II}}{8\mu\pi} \sqrt{2\pi r} \left[ (2\kappa + 3) \sin\left(\frac{\theta}{2}\right) + \sin\left(\frac{3\theta}{2}\right) \right] \quad (5)$$

$$u_y = \frac{K_I}{8\mu\pi} \sqrt{2\pi r} \left[ (2\kappa + 1) \sin\left(\frac{\theta}{2}\right) - \sin\left(\frac{3\theta}{2}\right) \right] - \frac{K_{II}}{8\mu\pi} \sqrt{2\pi r} \left[ (2\kappa - 3) \cos\left(\frac{\theta}{2}\right) + \cos\left(\frac{3\theta}{2}\right) \right] \quad (6)$$

[3]. Thus, individual  $K_I$  and  $K_{II}$  values can be solved by solving the system of equations with the known displacement values at any given point.

## 2.2 Procedure

The experiment was conducted with a thin rectangular polymethyl methacrylate (PMMA) specimen. To simulate a crack, the specimen was cut with a band saw in the center to a length of 25.4 mm. This method was chosen to allow for a blunt crack tip to prevent premature failure of the specimen while testing. One side of the plate was painted completely white and then speckled using a black aerosol paint. The paint was dispensed through a small electric fan to aid in the random dispersion of speckles onto the sample. A close up of the resulting speckle pattern can be seen in Figure 1.

To extract Mode I data, the specimen was placed into a symmetric three-point bend fixture within an electronic screw-driven universal testing machine (Instron, Norwood MA). A light load was used to hold the specimen in place while the DIC camera was adjusted (Correlated Solutions, Irmo SC). The DIC system consisted of one camera with a 35 mm lens mounted to a tripod and two adjustable green LED lights with flexible attachments. The camera and lights were set and adjusted according to the manufacturers recommendations [7]. The test setup with the DIC system in place is shown in Figure 1.

Several images were taken to obtain an initial reference and estimate unwanted noise. The load was then manually incremented in steps of approximately 100 N up to 1010 N. An image was taken at each increment. The same test procedure was repeated for the mixed mode loading configuration. Images were processed using an available commercial software Vic-2D (Correlated Solutions, Irmo SC).

## 2.3 Error and Uncertainties

DIC accuracy was evaluated using the built-in Vic-2D function [8]. Documentation establishes that an acceptable error metric is less than 0.05. The reported error values for all images were 0.006. The reported error is an average measure related to speckle pattern, subset size and quantity, focus, contrast, glare, and F-stop [9].

## 3 Results

In total, eight images were recorded and analyzed for each loading configuration. DIC was used to calculate  $u_x$  and  $u_y$  for each of the eight load increments. Rectangular sub-regions surrounding the crack were selected for analysis. Signal to Noise Ratio tended to decrease with increased load so analysis was focused on the 1010 N load increment. Equation 3 and Equation 4 were inverted to solve for  $K_I$  and experimental displacement fields were used to create contour plots of  $K_I$ , shown in Figure 4 and Figure 5. Inverting these equations created singularities as the denominator trended towards 0 at  $\theta = \pm\pi$ , so values exceeding  $2 MPa\sqrt{m}$  were eliminated to increase contrast.

Experimental  $K_I$  values were observed to be highly dependent on location.  $K_I$  became less accurate as distance from the crack increased for values calculated from  $u_x$  data. The opposite relation was observed for  $u_y$  data. To analyze how well theoretical  $K_I$  fit the experimental data, two points along the x-axis on the  $K_I^{u_x}$  plot were chosen for further analysis.  $K_I$  was then calculated for each of the eight load increments. Results are shown in Figure 6.  $K_I$  at both locations closely matched predicted values with  $R^2 > 0.98$  in both cases.

Contour plots of raw  $u_x$  and  $u_y$  displacement data were drawn and shown in Figure 7 and Figure 8. Quiver plots of combined displacement fields for Mode I dominant and mixed mode loading scenarios are shown in Figure 9 and Figure 10

Values of  $K_I$  and  $K_{II}$  were extracted from the mixed mode  $u_x$  and  $u_y$  displacement fields. A contour plot of the mode mix ratio surrounding the crack is shown in Figure 11.

## 4 Discussion

The general shape of both  $u_x$  and  $u_y$  fields in Mode I tests matched well with predictions. Field magnitudes also agreed closely, but spacing between contour lines did not always match perfectly. The roughness in experimental contours is likely due to errors inherent in DIC methods such as finite pixel/speckle size and subset selection. There are several possible explanations for disagreements in contour spacing. First, theoretical calculations depend on shear modulus,  $\mu$ , which was not measured, but derived from Young's Modulus and Poisson's ratio. Additionally, theoretical calculations assume an infinitely thin crack with a sharp tip. The test specimen crack was cut with a band saw and therefore has a finite width and a blunted tip.

Mixed mode testing produced less definitive results. Plots in Figure 9 and Figure 10 are very similar, although the slight asymmetry in the vectors of the mixed mode plot indicate that there is a small degree of mode mixity. When the two values are calculated and compared, it was shown that the mode mixing varied the most at the edge of the specimen, where  $K_I/K_{II}$  was approximately 5.5. Closer to the crack tip, the two stress intensity factors were about equal. The reason for the low level of mode mixity is likely a result of the load being placed over the crack in the mixed mode configuration. The shear was positive on both sides of the crack, although it was greater on the side above the crack. This difference in shear created the Mode II loading, although it was relatively low when compared to the magnitude of the Mode I load.

## 5 Conclusion

Displacement fields were compared for an edge crack in Mode I loading using both a closed form analytical solution and experimental data. These displacement fields were similar in magnitude, although the location of various contours did not match entirely. These displacements were used to calculate Mode I stress

intensity factors across a variety of loads. When compared with each other, these stress intensity factors agreed very well adjacent to the crack tip. These results demonstrate that LEFM is only valid in a select region around the crack. This region is dependent on geometry and loading configurations. When a mixed mode load configuration was applied to the specimen, the overall mode mix was still predominantly Mode I, although there was enough Mode II loading present that the respective stress intensity factors were able to be computed and compared. This test showed that DIC data combined with the Westergaard stress function solution produces accurate values for stress intensity factors under various loading configurations.

## 6 Figures

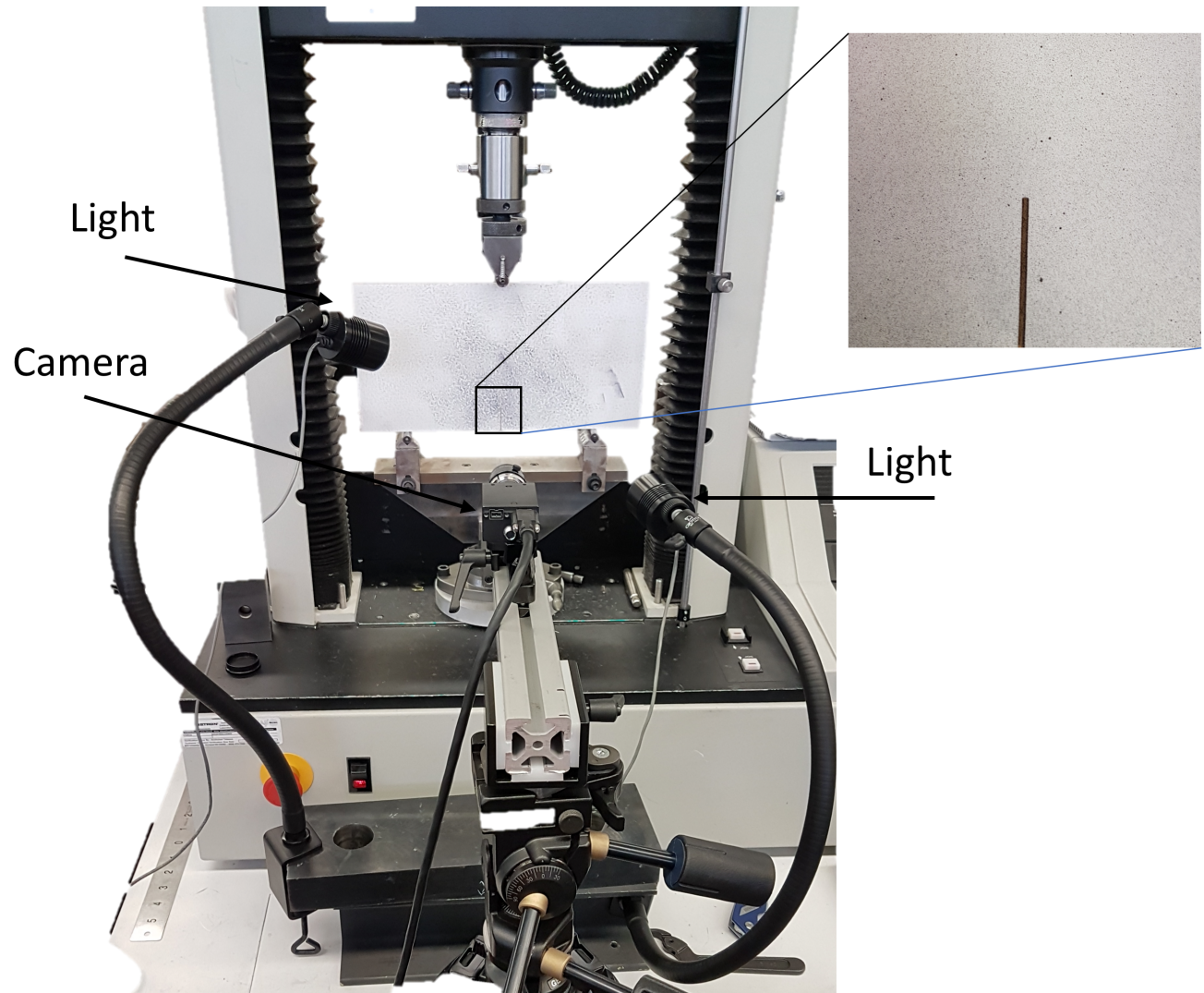


Figure 1: Experimental setup with close up of speckle pattern

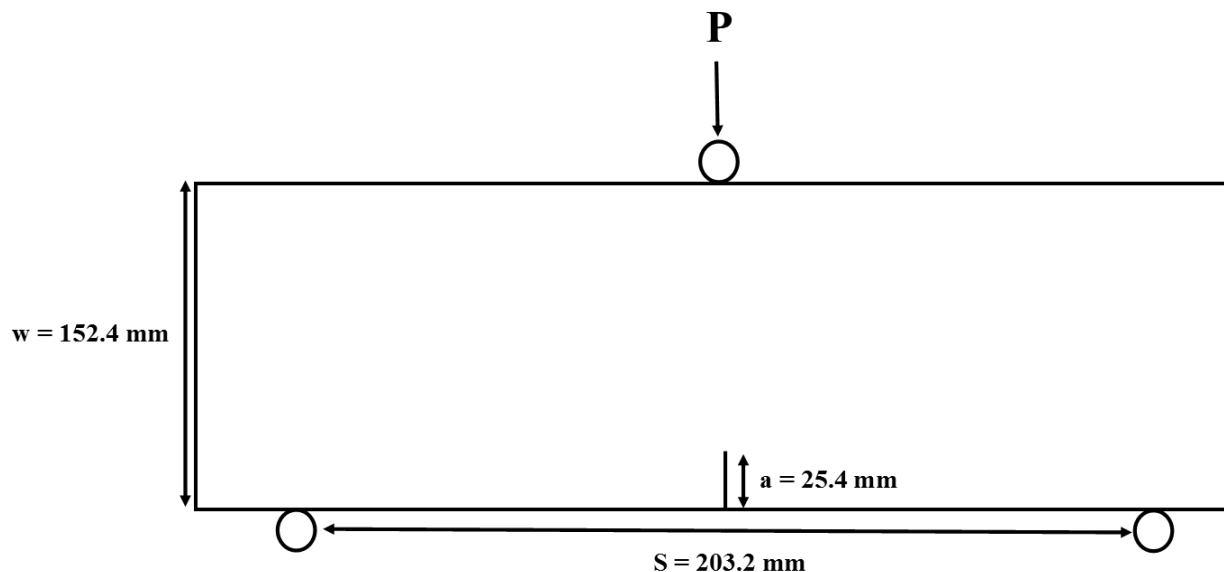


Figure 2: Single Edged Notch Bend specimen, where thickness  $B = 8.75 \text{ mm}$ . Applied load,  $P$ , is applied to the top roller

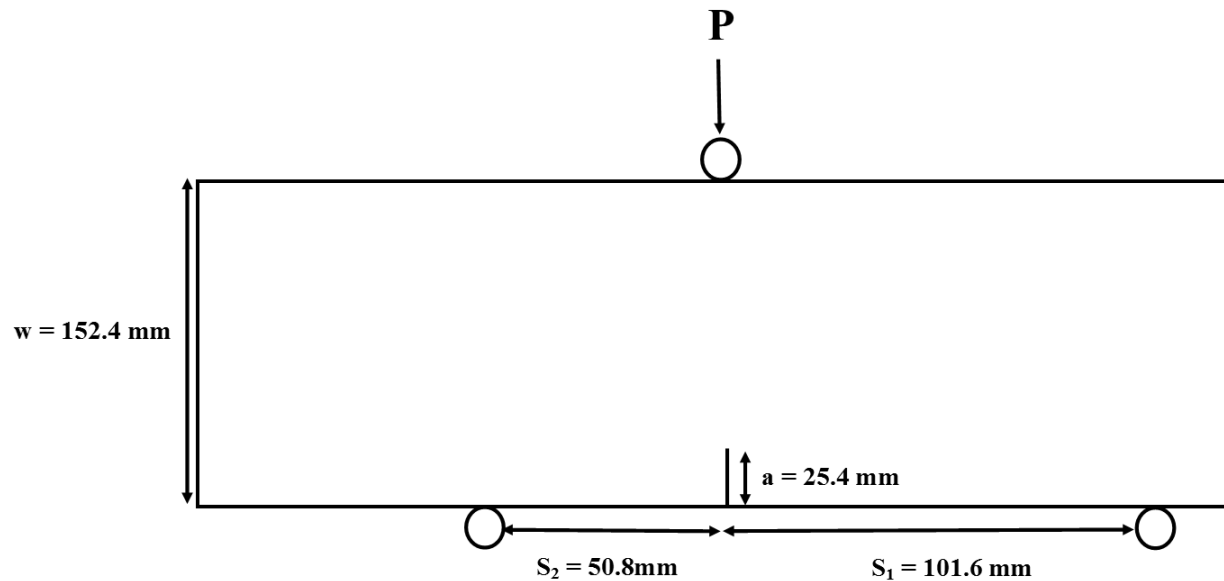


Figure 3: Mixed mode Single Edged Notch Bend specimen, where thickness  $B = 8.75 \text{ mm}$ . Applied load,  $P$ , is applied to the top roller

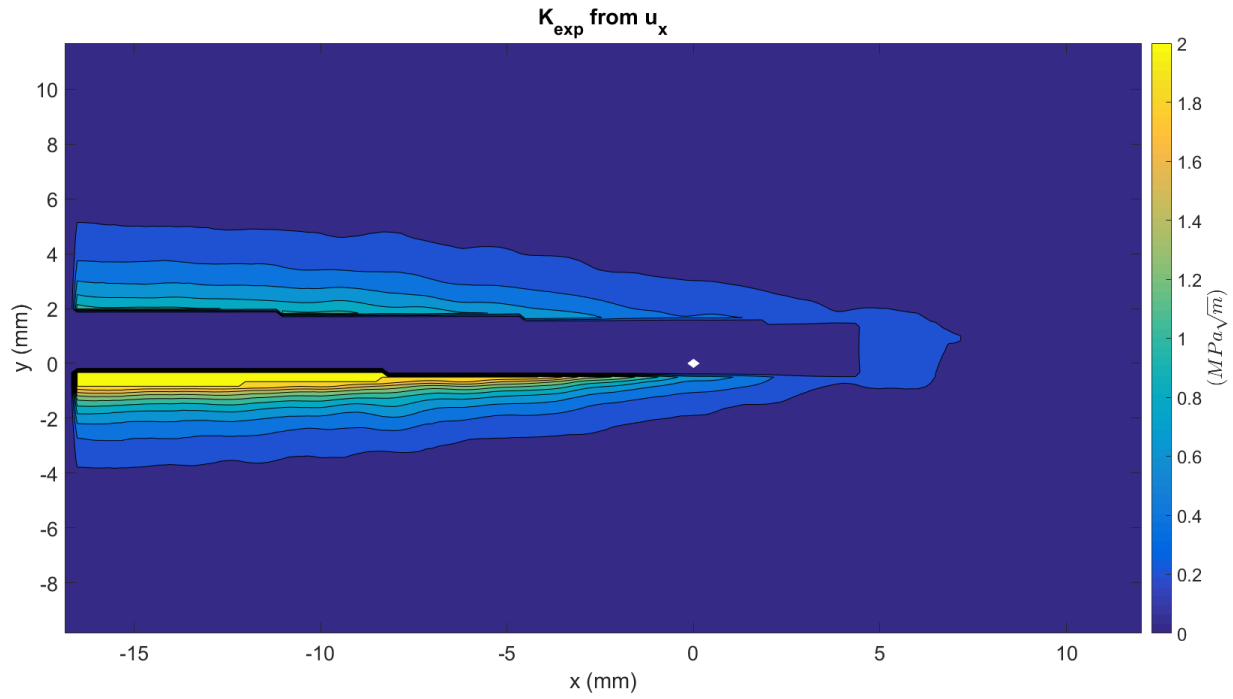


Figure 4: Contour plot of experimental values  $K_1^{u_x}$ . Values above  $2 \text{ MPa}\sqrt{m}$  have been set to 0 for clarity

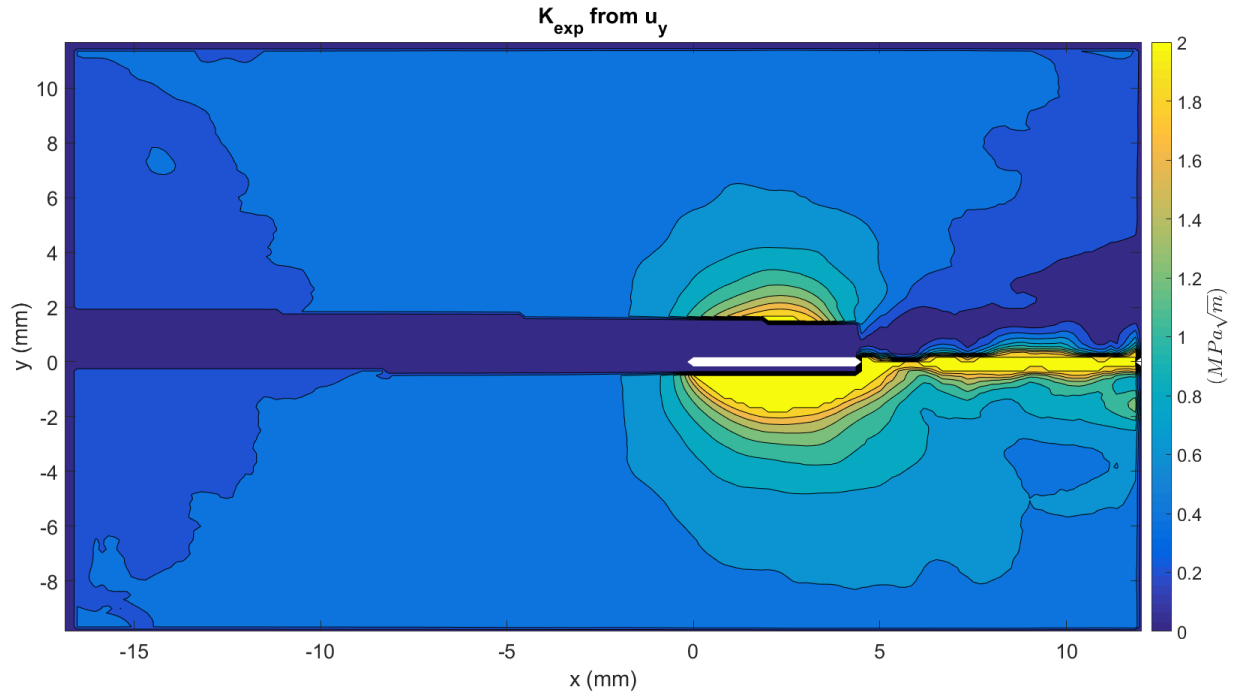


Figure 5: Contour plot of experimental values  $K_1^{u_y}$ . Values above  $2 \text{ MPa}\sqrt{m}$  have been set to 0 for clarity

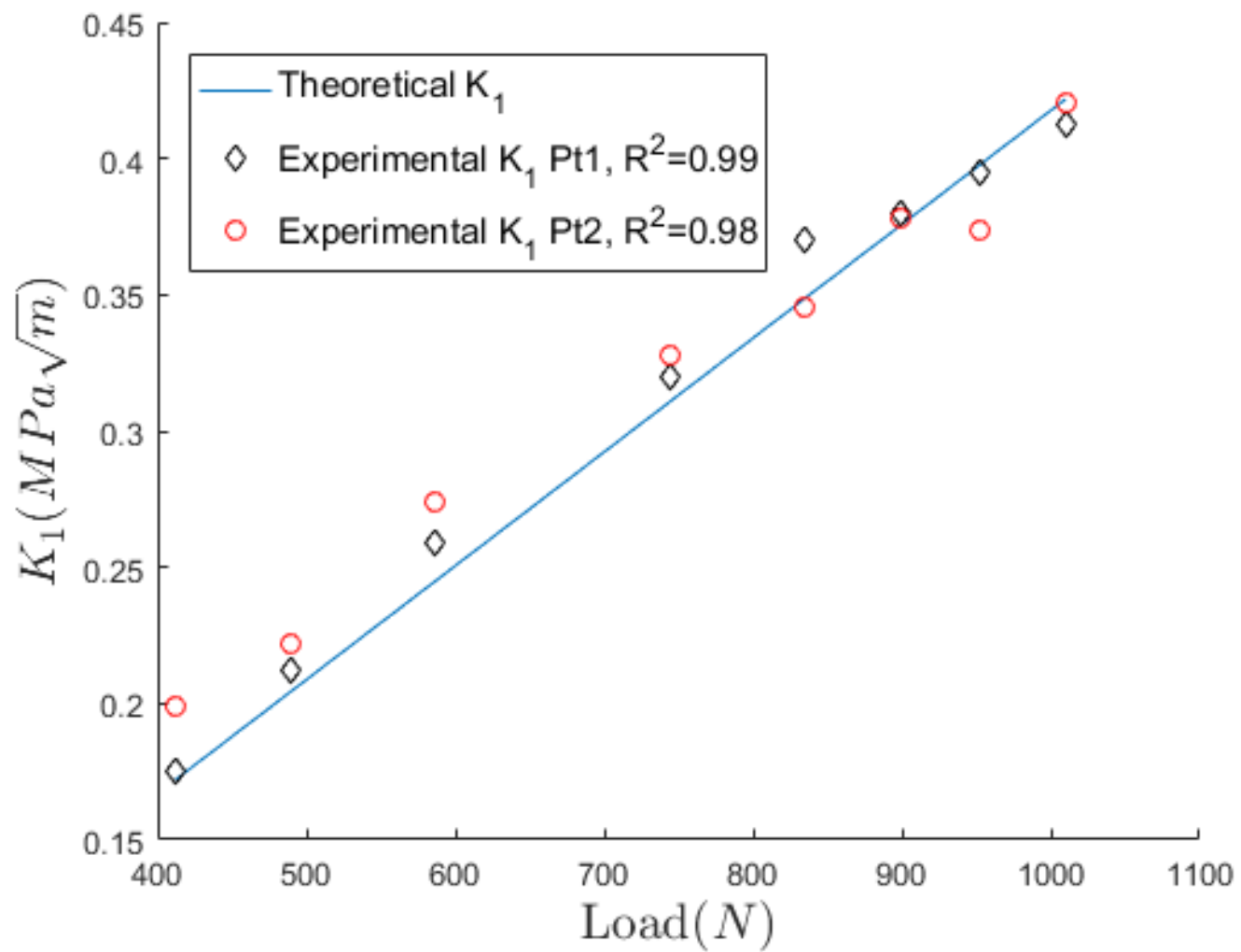


Figure 6: Theoretical and experimental Mode I stress intensity factor at two points along the x-axis.

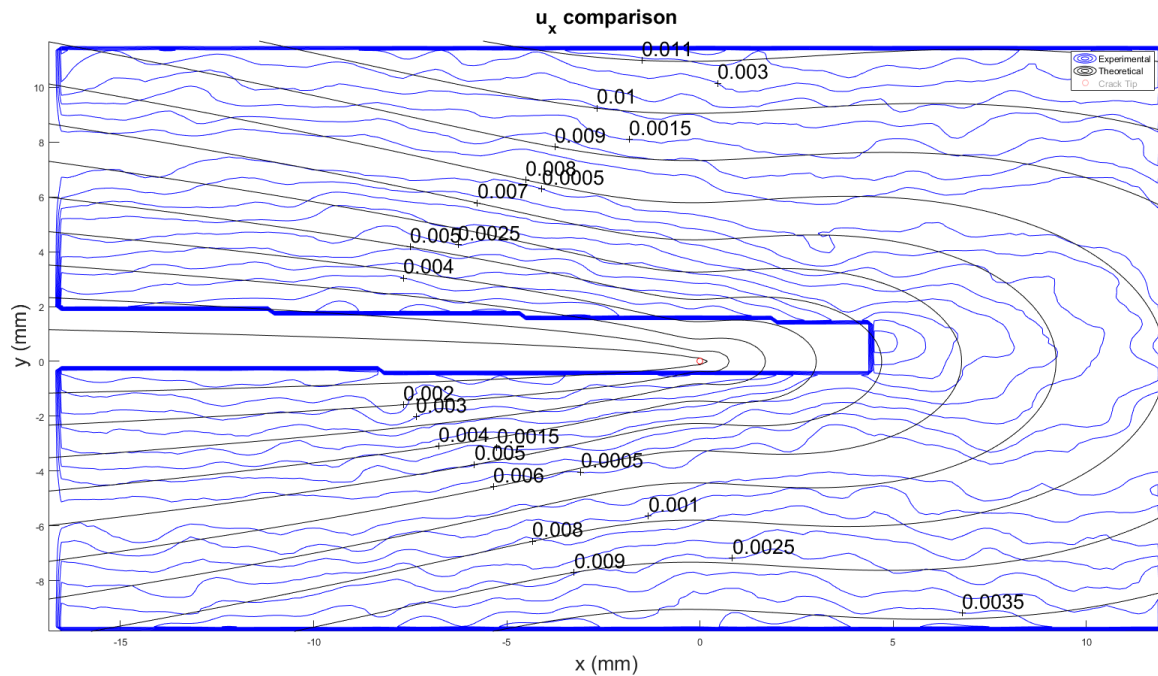


Figure 7: Comparison between theoretical and experimental  $u_x$  displacements

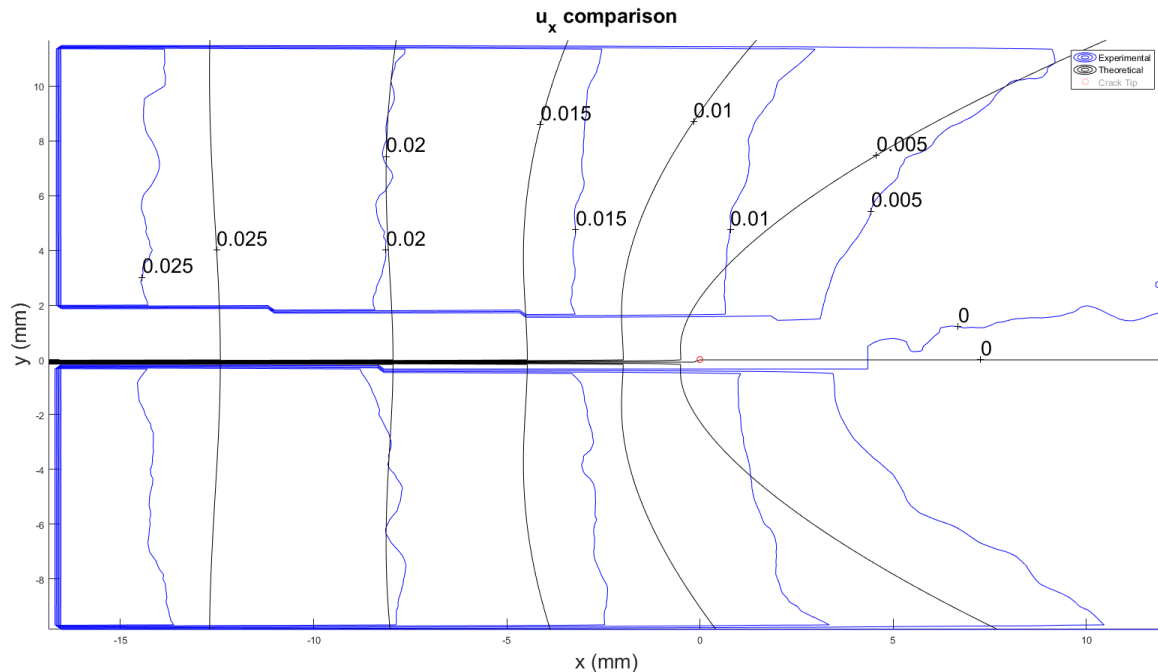


Figure 8: Comparison between theoretical and experimental  $u_y$  displacements

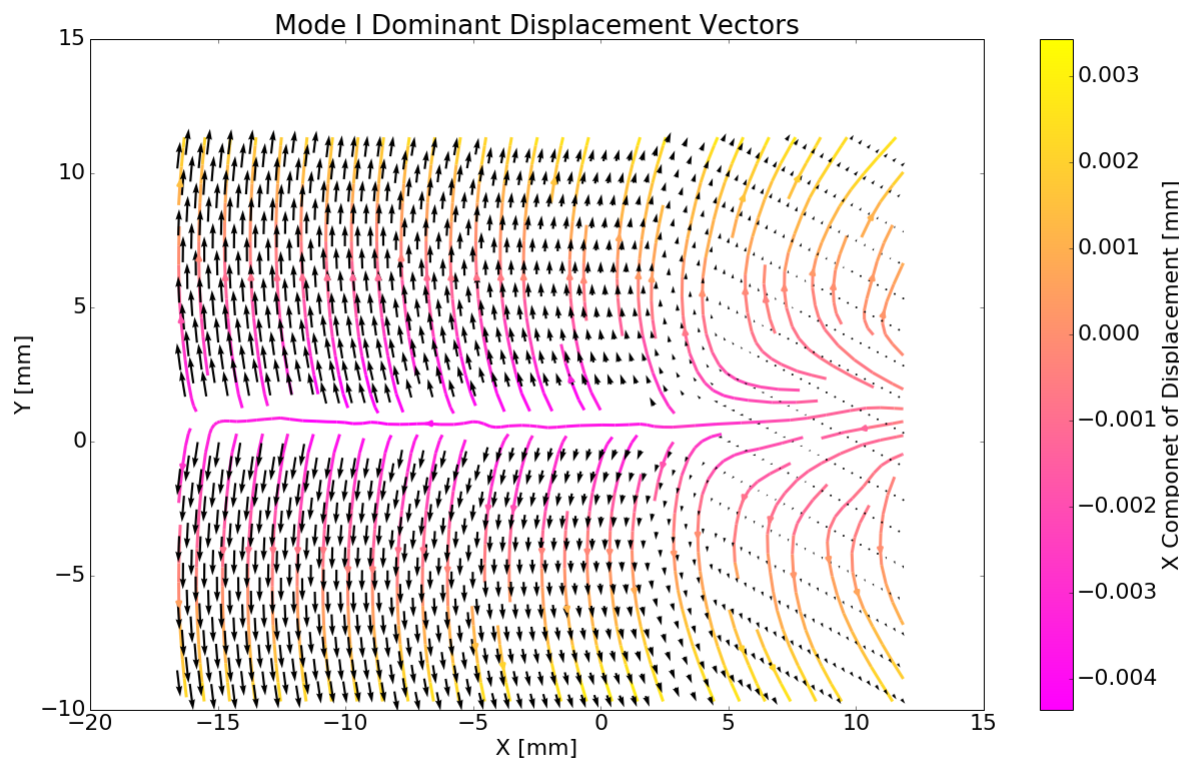


Figure 9: Displacements vectors around crack tip for a symmetric load of 534.7 N.

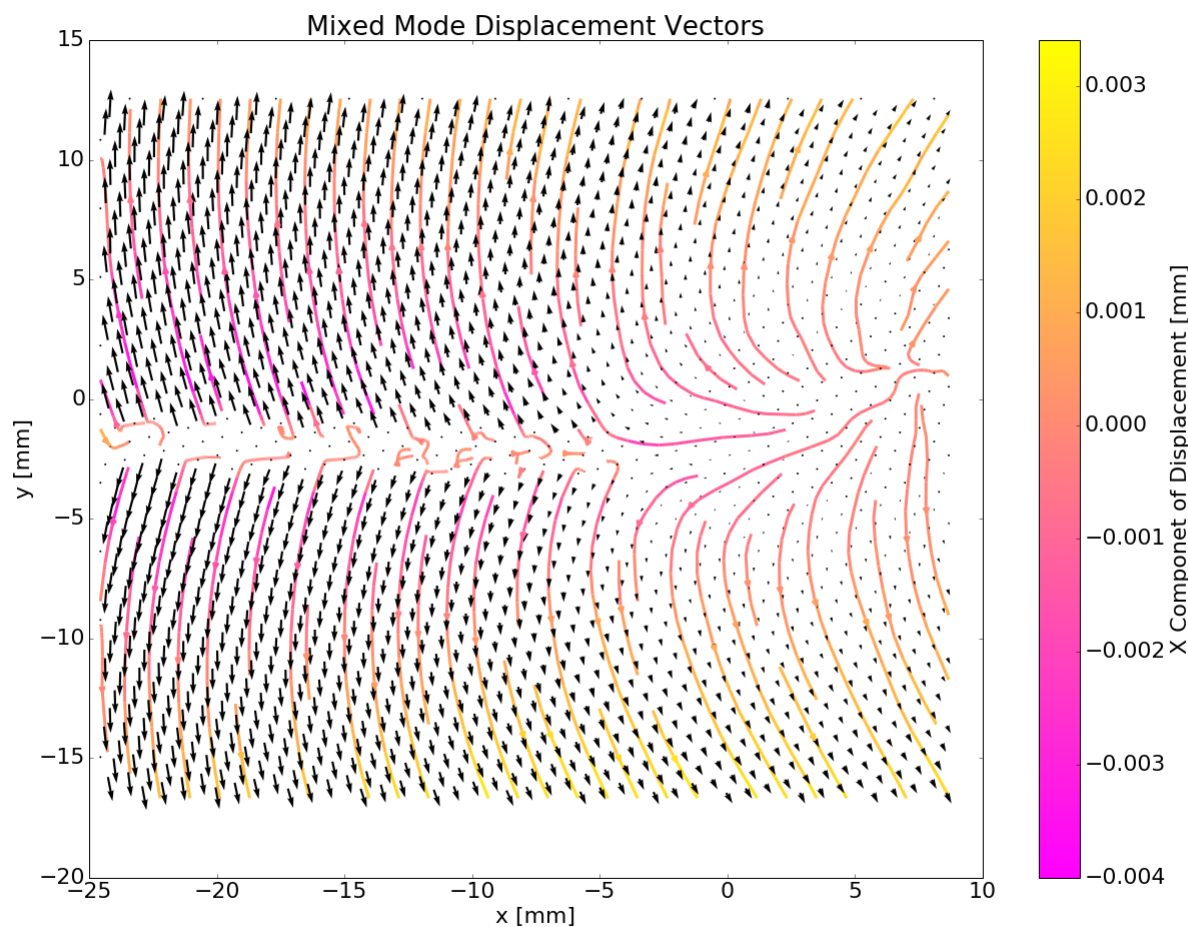
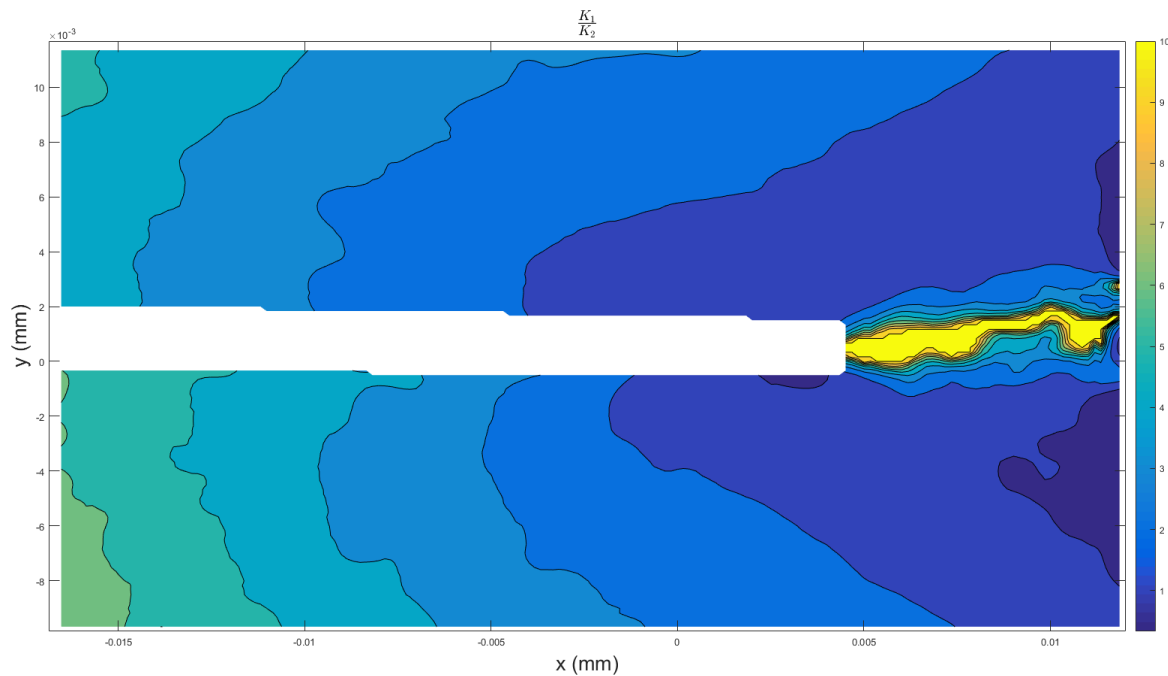


Figure 10: Displacements vectors around crack for an asymmetric load of 587 N.

Figure 11: Contour plot of  $K_I/K_{II}$

## References

- [1] E. T. Levend Parnast, Omer G. Bilir, "Strain gage methods for measurement of opening mode stress intensity factor," *Engineering Fracture Mechanics*, 1996.
- [2] L. H. Rui Zhang, "Measurement of mixed-mode stress intensity factors using digital image correlation-method," *Optics and Lasers in Engineering*, 2012.
- [3] T. Anderson, *Fracture Mechanics Fundamentals and Applications*, 3rd ed. CRC Press, 2005.
- [4] H. W. S. Michael A. Sutton, Jean-Jose Orteu, *Image Correlation for Shape, Motion and Deformation Measurements*. Springer, 2009.
- [5] S. B. H. S. J. V. D. V. H. A. H. D. Lecompte, A. Smiths, "Quality assessment of speckle patterns for digital image correlation," *Optics and Lasers in Engineering*, 2006.
- [6] G. I. H. Tada, P.C. Paris, *The Stress Analysis of Cracks Handbook*, 2nd ed. Paris Productions, 1985.
- [7] *Vic-2d v6 Testing Guide*, Correlated Solutions.
- [8] *Vic-2D Reference Manual*, Correlated Solutions.
- [9] *Minimizing Noise And Bias in 3D DIC*, Correlated Solutions.